

Task-conditioned Ensemble of Expert Models for Continuous Learning

Renu Sharma, Debasmita Pal, Arun Ross
Michigan State University, USA

sharma90@msu.edu, paldebas@msu.edu, rossarun@cse.msu.edu

Abstract

One of the major challenges in machine learning is maintaining the accuracy of the deployed model (e.g., a classifier) in a non-stationary environment. The non-stationary environment results in distribution shifts and, consequently, a degradation in accuracy. Continuous learning of the deployed model with new data could be one remedy. However, the question arises as to how we should update the model with new training data so that it retains its accuracy on the old data while adapting to the new data. In this work, we propose a task-conditioned ensemble of models to maintain the performance of the existing model. The method involves an ensemble of expert models based on task membership information. The in-domain models—based on the local outlier concept (different from the expert models) provide task membership information dynamically at run-time to each probe sample. To evaluate the proposed method, we experiment with three setups: the first represents distribution shift between tasks (LivDet-Iris-2017), the second represents distribution shift both between and within tasks (LivDet-Iris-2020), and the third represents disjoint distribution between tasks (Split MNIST). The experiments highlight the benefits of the proposed method. The source code is available at [GitHub](#).

Keywords— domain incremental learning, iris presentation attack detection

1. Introduction

While much of the research in machine learning focuses on achieving higher accuracy in various classification and regression tasks, maintaining that level of performance in non-stationary environments [32] remains a relatively underexplored area. Non-stationary environments arise from factors such as changes in sensors, location, population groups, and other variables. These changes lead to distribution shifts—shifts in input and output distributions or their relationships—that degrade model performance [8, 23, 32]. To sustain the performance of deployed models, it is essential to enable continuous learning with new task data while

retaining knowledge from previous tasks.

One straightforward solution for continuous learning is to fine-tune the model with new data. However, this often leads to catastrophic forgetting of previously learned tasks [8, 15, 23]. Another option is to retrain the model using a comprehensive dataset that includes both old and new data. However, in real-world applications, old training data is often unavailable due to security, privacy, or operational constraints. Several continuous learning approaches [50], such as regularization-based [2, 20], replay-based [3, 16], optimization-based [12, 24], representation-based [33, 52], and architecture-based [11, 55] methods, have been proposed in the literature. Most of these strategies aim to learn all subsequent tasks using a shared set of parameters (i.e., a single model), which can lead to significant inter-task interference [9, 29, 36]. This challenge becomes even more pronounced as the number of tasks increases, placing the entire burden on a single model.

We propose a multi-model approach in which each model is responsible for a specific task (an expert model), and the final score is obtained by dynamically merging the scores of these expert models based on their task membership information. We consider a practical scenario where task information is not explicitly provided, but sufficient task-specific data is available to either train an expert model or utilize an already available expert model. Unlike previous methods [16, 20, 24, 55], which often involve updating the training data, strategies, or architecture of expert models, our approach does not interfere with the training process of the expert models. Instead, we offer a framework that enables the reuse of existing expert models, each tailored to a particular task. Our main contributions are as follows:

1. We propose an ensemble of expert models, where the final prediction is obtained by combining scores from individual expert models based on task membership information.
2. We introduce an in-domain model that dynamically estimates task membership information for each probe sample, using the concept of local outlier detection.
3. We validate the effectiveness of our method through experiments on three diverse setups, each capturing different

types of distribution shifts: LivDet-Iris-2017 (distribution shifts between tasks), LivDet-Iris-2020 (distribution shifts both between and within tasks), and Split MNIST (disjoint distributions between tasks).

2. Related Work

Continuous learning encompasses three scenarios [14, 46]: Task-Incremental Learning (Task-IL), Domain-Incremental Learning (Domain-IL), and Class-Incremental Learning (Class-IL). Task-IL involves incrementally learning several independent tasks, with explicit knowledge of the task identity. Domain-IL focuses on learning tasks from the same output class-label space, but with varying input distributions, and without task identity. Class-IL, on the other hand, involves incrementally learning new classes in each task, without any information about the task identity. In this work, we focus on the Domain-IL scenario for continuous learning.

In the literature, continuous learning methodologies are typically categorized into five main groups [50]: regularization-based, replay-based, optimization-based, representation-based, and architecture-based approaches. Regularization-based approaches introduce additional constraints to the learning process, penalizing drastic changes in model parameters [2, 20, 21, 23, 37, 39, 57, 58]. Replay-based approaches enhance existing expert models with memory mechanisms to retain information about previously learned tasks [3, 6, 16, 27, 34, 42, 45, 53]. Optimization-based techniques focus on explicitly designing or manipulating optimization algorithms, such as using gradient projection in the gradient or input space of old tasks [12], meta-learning for sequentially arriving tasks within the inner loop, and exploiting mode connectivity and flat minima in the loss landscape [24, 31]. Representation-based approaches leverage the strengths of learned representations, including sparse representations from meta-training [17], self-supervised learning (SSL) [28, 33], and large-scale pre-training [41, 52]. Architecture-based approaches involve task-specific or adaptive parameters within a well-designed architecture, such as assigning dedicated parameters to each task (parameter allocation) [19, 55], constructing task-adaptive sub-modules or subnetworks (modular networks) [35, 38], and decomposing the model into task-sharing and task-specific components (model decomposition) [11, 54].

In the model decomposition category of architecture-based approaches, ensembles or multiple networks are used for continuous learning. Doan et al. [9] utilized ensembles of models and made them computationally efficient by leveraging neural network subspaces. The Model Zoo approach [36], inspired by boosting, grows an ensemble of small models, each trained during one episode of continuous learning. CoSCL [49] fixed the number of narrower

sub-networks to learn all incremental tasks in parallel and encouraged cooperation among them by penalizing the differences in predictions made by their feature representations. MERLIN [18] assumed that the weights of a neural network for solving any task come from a meta-distribution, which they learned incrementally. The CoMA [29] method selectively weights each parameter in the weight ensemble by leveraging the Fisher information of the model’s weights. Lee et al. [22] proposed a closely related approach, where they learned separate expert models for each task and measured the marginal likelihood of the expert models using a density estimator. In contrast, our method dynamically assigns task membership information to expert models using an in-domain model.

3. Proposed Approach

In this work, we propose a task-conditioned ensemble framework of expert models that preserves performance across all learned tasks. Figure 1 illustrates the proposed approach. Consider a scenario with two tasks (Task 1 and Task 2). For Task 1, we use its corresponding expert model for inference, while simultaneously training an in-domain model. For Task 2, we train separate expert and in-domain models specific to Task 2’s training data. During inference, we combine the predictions from the expert models using their respective in-domain models. These in-domain models provide membership information for the probe sample, indicating the task it belongs to. Importantly, probe samples can come from any task, without revealing the task identity. In other words, the in-domain model estimates the task identity of a probe sample. The final prediction score for Task 2 is calculated as follows:

$$s = s_1 \cdot m_1 + s_2 \cdot m_2 \quad (1)$$

where, s_1 and s_2 are prediction scores from expert models, and m_1 and m_2 are membership scores from in-domain models.

Our main contribution lies in the introduction of the in-domain model, which estimates membership scores. The in-domain model operates on the principle of outlier detection: for each probe sample, it determines the degree to which the sample is an outlier with respect to the training distributions. To achieve this, the in-domain model consists of two components: (i) a *feature extractor* that represents task-specific data in feature space, and (ii) a *distance measure* that provides a membership score based on the outlier score of the probe sample relative to the task-specific feature space. The details of these components are as follows.

Feature Extractor (FE): The base architecture we use for feature extraction is a Vision Transformer (ViT) [10]. The success of transformers in natural language processing [48] and computer vision [10] inspired us to adopt them for

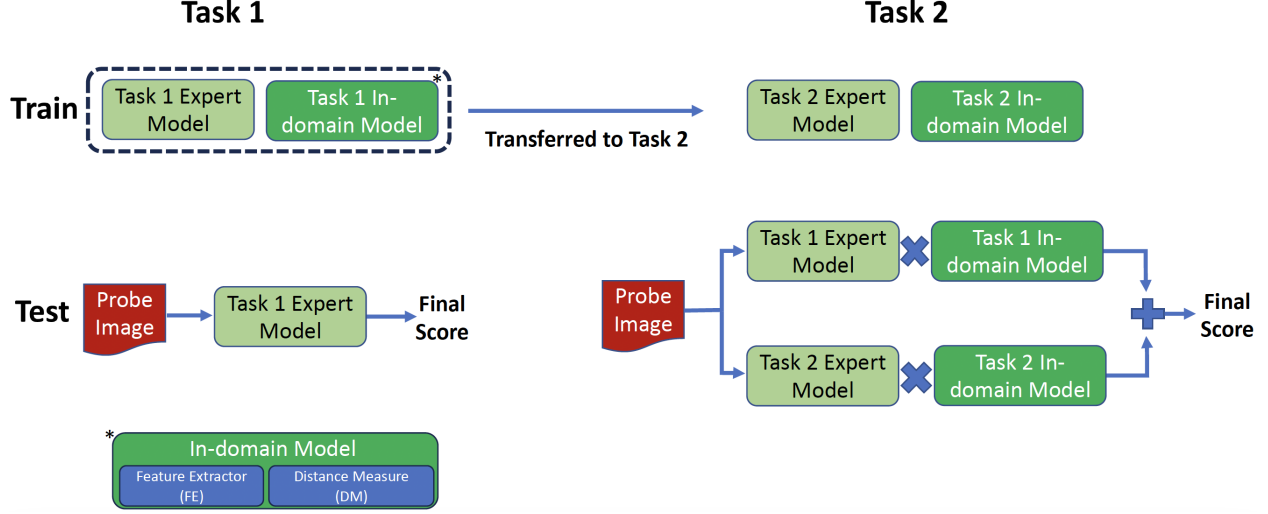


Figure 1. The overall idea of the task-conditioned ensemble of models of continuous learning. Task 1 inference utilizes its only expert model, whereas task 2 inference utilizes both expert models with the help of in-domain models that provide membership information. In-domain model consists of two components: Feature Extractor (FE) and Distance Measure (DM).

representing task-specific data. While convolutional neural networks (CNNs) capture local structures in images, they are less effective at modeling global information. In contrast, ViT excels at modeling global contextual information through its self-attention mechanism, making it highly suited for representing task-level information [30]. We train the ViT feature extractor using two losses: the center loss and the mean-shifted intra-class loss. The details of these losses are as follows:

1. Center Loss: The objective of the center loss is to extract features from the training data such that all feature embeddings get closer to the center of the embeddings. The center of the training data embeddings is calculated as

$$c = \mathbb{E}_{x \in \chi_{train}} [\phi(x)] \quad (2)$$

where, x is the input image, $\phi(x)$ is the feature embedding from the ViT model, and χ_{train} is the train set. The c is initialized with pre-trained ViT features. Thereafter, it gets updated in each epoch. The center loss is then calculated as

$$\ell_{center}(x) = \|\phi(x) - c\|^2. \quad (3)$$

The loss reduces the intra-train set variations among training data and forms a closer feature space for the samples. This helps in detecting outlier samples in presence of other task data.

2. Mean-Shifted Intra-Class Loss: The objective of this loss is to form a cluster of samples belonging to the same class around the center of feature embeddings. To accomplish the objective, we first mean-shifted the embeddings of the training samples as

$$\theta(x) = \frac{\phi(x) - c}{\|\phi(x) - c\|^2} \quad (4)$$

where, $\phi(x)$ is the feature embedding of input sample x and c is the center of the feature embeddings. We then estimate contrastive loss over the mean-shifted embeddings. Let x_{i1} and x_{i2} be two input images belonging to the same class C_i , then loss is defined as:

$$\begin{aligned} \ell_{msic}(x_{i1}, x_{i2})_{\{x_{i1}, x_{i2}\} \in C_i} &= \ell_{con}(\theta(x_{i1}), \theta(x_{i2})) \\ &= -\log \frac{\exp((\theta(x_{i1}) \cdot \theta(x_{i2}))/\tau)}{\sum_{j \neq i}^{2N} \exp((\theta(x_{i1}) \cdot \theta(x_j))/\tau)} \end{aligned} \quad (5)$$

where, $\theta(\cdot)$ is the mean-shifted embedding, N is the batch size, and τ is the temperature hyperparameter. Together, the two losses create a feature space where samples from the same class form a cluster close to the center of the training data. The class cluster formation helps in the detection of local outliers. By local outlier, we refer to a sample that has a low distance to the center of the training set but is an outlier with respect to other class distributions. Consider Figure 2, where the blue-colored data points represent the training set, C is the center of the training set, and the red-colored point P is a probe sample. There are two classes (Class 1 and Class 2) with different densities in the training set. If we consider the global outlier concept (measured by the distance to the center of the training set), the probe sample P would be an inlier to the blue-colored training set since its distance to the center is smaller compared to the data points of Class 1 and Class 2. However, according to the concept of local outlier, P is an outlier with respect to both Class 1 and Class 2 because the distance between data points within Class 1 or Class 2 is smaller than the distance between the probe sample and the data points of Class 1 or Class 2. As a result, the probe sample P is considered an outlier with respect to the entire blue-colored training

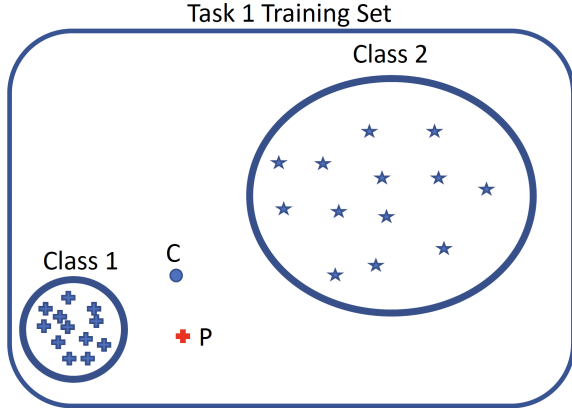


Figure 2. Illustration of a local outlier concept, motivation for defining feature space. Blue-colored data points belong to one training set; C is the center of the training set; and red-colored data point P is a probe sample. There are two classes (Class 1 and Class 2) in the blue-colored training set. If we consider the global outlier concept, the red-colored probe sample would be an inlier. However, if the local outlier concept is used, the probe sample is an outlier to both Class 1 and Class 2 as well as to the blue-colored training set. The figure is better viewed in color.

set. Therefore, the local outlier concept is more effective for membership assignment because it focuses not only on the overall task distribution but also on the class distribution within each task.

The total loss used to train the feature extractor is the sum of center loss and mean-shifted intra-class loss:

$$\ell_{total}(x', x'') = \ell_{center}(x') + \ell_{center}(x'') + \ell_{msic}(x', x''). \quad (6)$$

Distance Measure (DM): After representing the training data and the probe sample, we estimate the distance of the probe sample with respect to the training data using the Local Outlier Factor (LOF) [5]. LOF is a density-based local outlier detection technique that identifies anomalous points relative to a local cluster of neighboring points by incorporating a nearest-neighbor algorithm. It detects outliers whose density is significantly lower than that of their neighbors. The losses we proposed to represent the training data help in estimating the local outliers using LOF. If the LOF score is approximately 1, it suggests that the sample has a density similar to that of its neighbors. A score less than 1 indicates that the sample has a higher local density than its neighbors, while a score greater than 1 indicates that the sample has a lower density than its neighbors. To assign a membership score to each expert model, we first invert the LOF scores (l_1, l_2) and then apply SoftMax normalization, as follows:

$$(m_1, m_2) = softmax\left(\frac{1}{l_1}, \frac{1}{l_2}\right). \quad (7)$$

4. Experimental Setup and Results

To evaluate the proposed method, we conduct experiments across three setups: LivDet-Iris-2017, LivDet-Iris-2020, and Split MNIST. The LivDet-Iris-2017 and LivDet-Iris-2020 setups involve two tasks in sequence, while the Split MNIST setup involves five tasks in sequence. The LivDet-Iris-2017 setup represents a scenario where a distribution shift occurs between tasks, but no shift occurs within a task (except in one case, explained in Section 4.1). The LivDet-Iris-2020 setup illustrates a scenario where distribution shifts occur both between and within tasks. The Split MNIST setup represents a scenario where the distributions of different tasks are disjoint, but there is no shift within tasks. The LivDet-Iris-2017 and LivDet-Iris-2020 setups reflect practical scenarios in the application of presentation attack (PA) detection, i.e., spoof detection, for iris biometric recognition systems. In this case, PA detection is treated as a binary classification problem, distinguishing between bonafide iris images and PA images (such as prints, cosmetic contact lenses, artificial eyes, and electronic displays). The Split MNIST setup is a simulated continuous learning scenario, used to compare the proposed method with existing state-of-the-art (SOTA) continuous learning techniques.

For training the feature extractor (FE) model, we initialize the weights from a pre-trained ViT-Base model [10] trained on the ImageNet-21k and JFT-300M datasets. We remove the MLP head used for classification from the original ViT architecture to make it a feature extractor. We use 100 epochs, a batch size of 15, 0.25 as the value of τ and the stochastic gradient descent (SGD) optimizer with a learning rate of $1e-5$. For the implementation of the LOF distance measure, we use the default values provided in [5], 20 as the number of neighbors, and the Euclidean distance as the distance metric.

4.1. LivDet-Iris-2017 Setup and Results

In this setup, we use two datasets: a proprietary dataset and the LivDet-Iris-2017 dataset [56]. The proprietary dataset is used for Task 1, and the LivDet-Iris-2017 dataset is used for Task 2. The proprietary dataset and expert models are taken from [40]. The LivDet-Iris-2017 dataset [56] is a publicly available dataset for iris presentation attack (PA) detection. It consists of four subsets: Clarkson, Warsaw, Notre Dame, and IIITD-WVU. Each subset contains corresponding training and test sets. The Warsaw and Notre Dame test sets are further split into known and unknown test splits based on types of PAs included in the test set with respect to the training set. The Clarkson and Notre Dame test sets correspond to the cross-PA scenario, while the Warsaw data represent a cross-sensor scenario. The IIITD-WVU subset represents a cross-dataset scenario where a distribution shift also occurs within the task. Table 1 summarizes the training and

Table 1. Description of the task 1 and 2 training/test sets in the LivDet-Iris-2017 setup along with the number of bonafide and fake iris images present in the datasets. Each test set represents different testing scenarios. Here, ‘‘K. Test’’ means a known test set of the dataset, and ‘‘U. Test’’ means an unknown test set as defined in [56]

| Domains | Task 1 Train and Test Sets (Proprietary Dataset) | | Task 2 Train and Test Sets (LivDet-Iris-2017 Dataset) | | | | | | | | | |
|------------|--|----------------------|---|-------|--------|---------|---------|------------|---------|---------|-----------|-------|
| | Proprietary Split I | Proprietary Split II | Clarkson | | Warsaw | | | Notre Dame | | | IIITD-WVU | |
| Train/Test | Train | Test | Train | Test | Train | K. Test | U. Test | Train | K. Test | U. Test | Train | Test |
| Bonafide | 9,660 | 2,963 | 2,469 | 1,485 | 1,844 | 974 | 2,350 | 600 | 900 | 900 | 2,250 | 702 |
| PA | 6,075 | 352 | 2,468 | 1,673 | 2,669 | 2,016 | 2,160 | 600 | 900 | 900 | 4,000 | 3,507 |

Table 2. The performance of all methods in terms of True Detection Rate (% , higher the better) at 0.2% False Detection Rate on task 1 and 2 test sets of the LivDet-Iris-2017 setup.

| Test Sets | Task 1 | Task 2 | Task 1 | Task 2 | Task 1 | Task 2 | Task 1 | Task 2 | Task 1 | Task 2 |
|---|--------------|--------------|--------------|------------|-------------|--------------|-------------|--------------|--------------|--------------|
| | Proprietary | Clarkson | Proprietary | Warsaw | Proprietary | Notre Dame | Proprietary | IIITD-WVU | Proprietary | IIITD-WVU |
| Datasets | Test | Test | Test | K. Test | U. Test | Test | K. Test | U. Test | Test | Test |
| Task 1 Expert Model | 98.44 | 28.63 | 98.44 | 92.95 | 98.56 | 98.44 | 93.55 | 91.00 | 98.44 | 42.91 |
| Task 2 Expert Model | 25.54 | 92.05 | 0.31 | 100 | 100 | 29.90 | 100 | 66.55 | 0.31 | 29.30 |
| Fine-Tuned | 86.91 | 93.51 | 45.48 | 100 | 100 | 98.75 | 100 | 99.77 | 83.17 | 48.85 |
| Full-Retrain | 96.57 | 91.63 | 93.76 | 100 | 100 | 96.57 | 100 | 100 | 96.57 | 66.81 |
| Ensemble of Task 1 and 2 Expert Models | | | | | | | | | | |
| Equal Membership | 97.50 | 89.67 | 97.81 | 99.45 | 100 | 99.37 | 99.88 | 96.22 | 98.44 | 43.62 |
| Pre-trained ViT-DM | 98.13 | 72.80 | 91.27 | 100 | 99.38 | 99.37 | 100 | 80.44 | 88.16 | 29.27 |
| FE-DM (Proposed Method) | 98.44 | 92.67 | 98.13 | 100 | 100 | 99.37 | 100 | 99.55 | 98.13 | 44.94 |

test sets for both tasks, along with the number of images present in each set.

For comparison, we use the following methods: (i) **Task 1 Expert Model**: trained only on Task 1, (ii) **Task 2 Expert Model**: trained only on Task 2, (iii) **Fine-Tuned**: trained on Task 1 and then fine-tuned on Task 2, (iv) **Full-Retrain**: trained on both Task 1 and Task 2, (v) **Equal Membership**: ensemble of both expert models with equal membership, (vi) **Pre-trained ViT-DM**: ensemble of both expert models with dynamic membership, where the in-domain model uses a pre-trained ViT model for feature representation, and (vii) **FE-DM (Proposed Method)**: ensemble of both expert models with dynamic membership, where the proposed feature extractor (FE) model is used to represent the task data. Table 2 presents the performance of all the models in terms of True Detection Rate (TDR(%)) at a 0.2% False Detection Rate (FDR), as commonly used in the iris PA detection literature [40]. TDR represents the percentage of PA samples correctly detected, while FDR denotes the percentage of bonafide samples incorrectly detected as PA. Performance scores are reported individually for both Task 1 and Task 2 test splits. The goal is to achieve high performance (higher TDR) on both splits. The Full-Retrain model serves as an upper benchmark for evaluating the performance of continuous learning methods.

The Task 1 and Task 2 expert models perform well on their respective test splits but fail on the other task’s test split. The Fine-Tuned model performs well on Task 2 but suffers from catastrophic forgetting, resulting in poor performance on Task 1 test split. The Full-Retrain model performs well on both test splits but is not a practical solution, as old training data is often unavailable in real-world scenar-

ios. For the ensemble methods, we use the Equal Membership method to highlight the importance of dynamic membership and the Pre-trained ViT-DM method to demonstrate the relevance of the proposed FE module. The proposed method outperforms Full-Retrain (except for the IIIT-WVU test split) and both ensemble-based approaches, validating that the proposed FE model better represents the task data and that memberships are appropriately assigned to their respective expert models. We also visualize membership histograms for various test splits (Figure 3). These histograms show the membership scores assigned to the Task 2 expert model from both tasks’ test data. So membership scores closer to 0 indicate a higher priority for the Task 1 expert model, while scores closer to 1 indicate a higher priority for the Task 2 expert model. In all cases, the Task 1 test set receives higher scores for the Task 1 expert model, and the Task 2 test set receives higher scores for the Task 2 expert model, except for the IIIT-WVU split. The membership scores for the IIIT-WVU test set are around 0.5, as the distribution of the IIIT-WVU test set is independent of the training distributions of both tasks, which is expected behavior.

4.2. LivDet-Iris-2020 Setup and Results

In this setup, we utilize three datasets: the proprietary dataset, the Warsaw PostMortem v3 dataset [1], and the LivDet-Iris-2020 dataset [7]. We divide the proprietary dataset into three splits: one for the Task 1 training set and two for the Task 2 training sets. The Warsaw PostMortem v3 dataset is used as the third training split for Task 2, while the LivDet-Iris-2020 dataset serves as the test set, which exhibits a distribution shift from both Task 1 and Task 2 train-

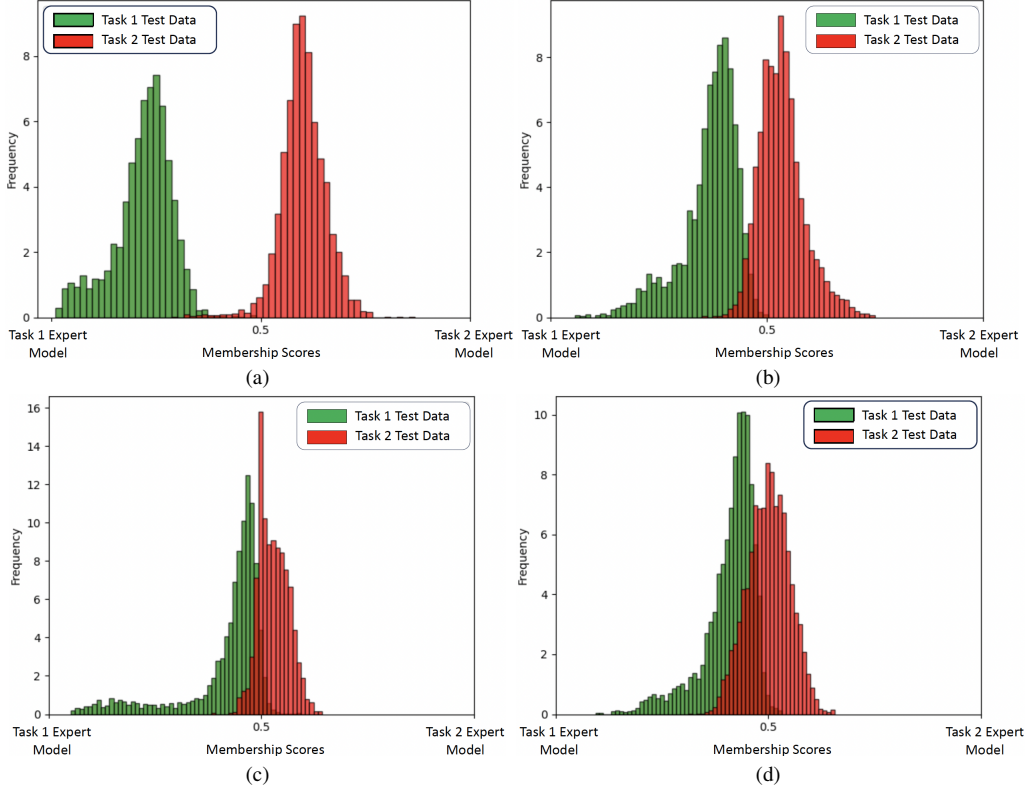


Figure 3. The histogram of membership scores assigned to all test samples (tasks 1 and 2) corresponding to (a) Clarkson, (b) Warsaw, (c) Notre Dame, and (d) IIIT-WVU subsets of the LivDet-Iris-2017 setup. In the case of Warsaw and Notre Dame, ‘Known’ test splits are used for illustration. Membership values toward ‘0’ on the x-axis symbolize higher priority given to the task 1 expert model, whereas membership values toward ‘1’ on the x-axis denote higher priority given to the task 2 expert model. The figure is better viewed in color.

ing sets. The different training splits for Task 2 correspond to no distribution shift, a cross-sensor shift, and a cross-PA shift. Table 3 details the number of bonafide and PA images used in these sets. Table 4 presents the performance of all the models in terms of TDR at a 0.2% False Detection Rate (FDR) on the LivDet-Iris-2020 test dataset.

The Task 1 and Task 2 expert models perform poorly on the test set, as its distribution differs from the training sets of both tasks. A similar issue occurs with the Fine-Tuned model. While the Full-Retrain model outperforms the other models, it is impractical due to the unavailability of the old training data. The proposed method, however, outperforms both ensemble methods (Equal Membership and Pre-trained ViT-DM) and achieves comparable performance to the Full-Retrain model.

4.3. Split MNIST Setup and Results

We also conduct experiments on the MNIST dataset to compare the proposed method with existing SOTA continuous learning strategies. The original dataset consists of 28×28 images of ten digits. We use the standard train-test split, with 60,000 training images and 10,000 test images. The primary task is to distinguish even-digit images from odd-

digit images, which is subdivided into five binary sub-tasks. The first task classifies the digits ‘0’ and ‘1’, the second task classifies ‘2’ and ‘3’, and so on. This dataset split is known as Split MNIST in the literature [14, 46]. The class labels remain consistent across all tasks. In this setup, the distributions of training data for different tasks are disjoint, but there is no shift between the training and test distributions within each task.

For a fair comparison, we use a multi-layer perceptron (MLP) architecture defined in [14] as the expert model. We compare the proposed method against Fine-Tuned, Full-Retrain, Equal Membership, Manual Membership, Pre-trained ViT-DM, and other SOTA continuous learning methods. In the Manual Membership approach, we manually assign a membership score of 1 to the correct expert model and 0 to the others. This method serves as an upper bound, as the training sets for all sub-tasks are disjoint. Table 5 presents the results of all methods.

The proposed method outperforms Fine-Tuned, ensemble-based methods, and other SOTA approaches. However, its performance is slightly lower than that of four replay-based methods: DGR [42], RtF [45], GEM [27], and ARI [51]. DGR [42], RtF [45], and ARI [51] are

Table 3. Description of the task 1 and 2 train/test sets in the LivDet-Iris-2020 setup, along with the number of bonafide and PA iris images present in the sets.

| Domains | Task 1 Train Set | | Task 2 Train Set | | | Test Set (Task 1 and 2) |
|------------|---------------------|----------------------|-----------------------|----------------------|----------|-------------------------|
| Datasets | Proprietary Split I | Proprietary Split II | Proprietary Split III | Warsaw PostMortem v3 | Combined | LivDet-Iris 2020 |
| Train/Test | Train | Train | Train | Train | Train | Test |
| Bonafide | 9,660 | 2,963 | 9,606 | - | 12,569 | 5,331 |
| PA | 6,075 | 352 | 922 | 2,400 | 3,674 | 7,101 |

Table 4. The performance of all methods in terms of True Detection Rate (% , higher the better) at 0.2% False Detection Rate on the LivDet-Iris-2020 test set.

| Domains | Task 1 | | Task 2 | | |
|--|--|----------------------|-----------------------|----------------------|--------------|
| Train Dataset | Proprietary Split I | Proprietary Split II | Proprietary Split III | Warsaw PostMortem v3 | Combined |
| Test Dataset | LivDet-Iris 2020 (Task 1 and 2 Test Set) | | | | |
| Task 1 and 2 Expert Models | 61.86 | 58.25 | 75.55 | 0.94 | 85.56 |
| Fine-Tuned | - | 63.18 | 66.53 | 0 | 83.00 |
| Full-Retrain | - | 77.96 | 76.96 | 67.76 | 94.05 |
| Ensemble of Task 1 and 2 Expert Models | | | | | |
| Equal Membership | - | 72.42 | 79.04 | 58.73 | 87.05 |
| Pre-trained ViT-DM | - | 69.91 | 79.03 | 58.73 | 89.38 |
| FE-DM (Proposed Method) | - | 69.27 | 81.36 | 61.99 | 93.62 |

Table 5. The average accuracy (% , higher the better) of the proposed approach with different SOTA continuous learning methods on the Split MNIST dataset. Methods with ‘+’ superscript are reported from [14], ‘o’ from [20], ‘*’ from [3] and ‘-’ from [22]. ARI [51] performance is reported from their own paper. All methods utilize the same experimental setup and expert models but differ in hyperparameters (batch size, learning rate, and number of epochs). We use the same hyperparameters as used in [14]. Each value is an average of ten runs.

| Method | Accuracy (%) |
|---|----------------|
| Fine-Tuned | 63.20 ± 0.35 |
| Full-Retrain | 98.59 ± 0.15 |
| EWC ⁺ [21] | 58.85 ± 2.59 |
| Online EWC ⁺ [39] | 57.33 ± 1.44 |
| SI ⁺ [58] | 64.76 ± 3.09 |
| KFAC ^o [37] | 67.86 ± 1.33 |
| MAS ⁺ [2] | 68.57 ± 6.85 |
| LwF ⁺ [23] | 71.02 ± 1.26 |
| OWM ^o [57] | 87.46 ± 0.74 |
| NCL ^o [20] | 91.48 ± 0.64 |
| BiC* [53] | 77.75 ± 1.27 |
| ER ⁻ [6] | 85.69 |
| GDumb* [34] | 88.51 ± 0.52 |
| RM* [3] | 92.65 ± 0.33 |
| DGR ⁺ [42] | 95.74 ± 0.23 |
| GEM ⁺ [27] | 96.16 ± 0.35 |
| RtF ⁺ [45] | 97.31 ± 0.11 |
| ARI [51] | 98.91 |
| Ensemble of Expert Models | |
| Equal Membership (Lower Limit) | 84.20 ± 0.08 |
| Manual Membership (Upper Limit) | 98.66 ± 0.008 |
| CN-DPM ⁻ [22] | 93.23 |
| Pre-trained ViT-DM | 81.34 ± 0.005 |
| FE-DM (Proposed Method) | 94.32 ± 0.01 |
| FE-DM with Mahalanobis Distance (Proposed Method) | 97.03 ± 0.0001 |

generative-based methods that involve training a separate generative model which is further used to augment the training of subsequent tasks. While this process improves performance, it also increases training time and makes the expert model dependent on the generative model. GEM [27] and ARI [51] methods also require additional memory to store a subset of the previous task samples, which raises concerns about both memory usage and privacy. ARI [51] further utilizes task identity during training. **However, the proposed method does not generate previous task samples, does not rely on task identity, and keeps the expert models independent from additional models.** The Manual Membership method achieves the highest performance (98.66%), surpassing all other methods, including the Full-Retrain method, and is comparable to ARI [51] (98.91%), highlighting the potential of ensemble-based approaches. When we experiment with an alternative distance measure, viz., Mahalanobis distance, it yields an accuracy of 97.03%, which is comparable to the highest performance. In this setup, Mahalanobis distance performs best, as the disjoint training distributions are effectively captured by the mean and variance, whereas LOF outperforms in the other setups. We also evaluate the forgetting behavior of our proposed approach (LOF as distance measure) using the Backward Transfer (BWT) metric [26], considering the sequential learning of tasks on Split MNIST dataset. We achieve a BWT of +0.9%. Typically, BWT is negative, indicating the extent of forgetting in previous tasks. However, the positive value in our case, suggests minimal forgetting, which could be attributed to our multi-model design that maintains independence across expert models.

To further emphasize the importance of our proposed FE module, we visualize the features extracted from pre-trained

ViT model (Figure 4a) and our trained FE model (Figure 4b) using t-SNE [47] (three dimensions). The features extracted by the pre-trained model exhibit significant overlap among the embeddings of different tasks, in contrast to the embeddings from our trained FE model, which are more distinct. Both the experimental results and the visualizations validate the effectiveness of the proposed loss functions in training the FE model.

4.4. Findings

The main findings from the three experimental setups are as follows:

1. When test distribution is similar to training data, the proposed method outperforms all the methods, including Full-Retrain, as shown in the LivDet-Iris-2017 setup (Table 2).
2. When there is a shift in test data distribution relative to all tasks' training data, the proposed approach still outperforms other methods and is comparable to the Full-Retrain method, as shown in the LivDet-Iris-2020 setup (Table 4).
3. In cases where the training distributions of different tasks are disjoint, the proposed approach outperforms Fine-Tuned, ensemble-based approaches, and various other SOTA methods. Its performance is lower than some of the replay-based methods, which could be improved using the Mahalanobis distance as a distance measure.
4. The proposed in-domain model effectively assigns membership scores to the respective expert models, leading to superior performance compared to the Equal Membership method as evident from the result in Tables 2, 4, and 5. The membership histograms in Figure 3 further validate the accurate allocation of membership scores.
5. The proposed FE model better represents the training data, as shown by its superior performance compared to the Pre-trained ViT-DM model in Tables 2, 4, and 5. The visual representation in Figure 4b further supports this finding.

5. Discussion on Memory Requirement and Scalability

Regarding memory requirements, the proposed method is more memory-efficient compared to other approaches, especially replay-based methods, as it does not have to store or transfer previous task images or features to subsequent tasks. Instead, the proposed method stores previous tasks' information in in-domain models (requires much lower memory than images/features). However, this setup raises concerns about scalability, when the number of models increases linearly with the number of tasks. To address this, the number of models can be reduced in several ways: (i) apply preconditions (such as performance or distribution shift measures) before building additional models; (ii) select a subset of expert/in-domain models based on prior knowledge of the test data; or (iii) merge expert and in-

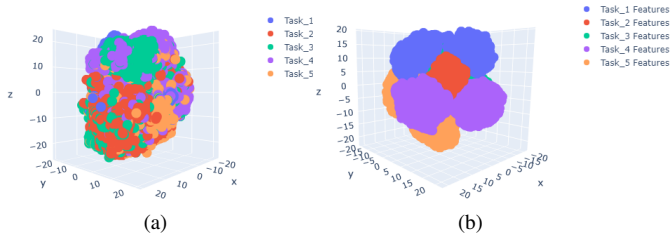


Figure 4. 3-D t-sne plots correspond to five sub-tasks of the Split MNIST dataset using (a) pre-trained ViT and (b) our trained ViT embeddings. Pre-trained ViT embeddings of different classes overlap with each other, whereas trained ViT embeddings form clusters of different classes. The figure is better viewed in color.

domain models using techniques like knowledge distillation [4, 25] or other methods [43, 44].

To address the scalability issue, we conducted a small experiment where we merged expert models using knowledge distillation [13]. For this experiment, we considered the first three consecutive sub-tasks of the Split MNIST dataset (Section 4.3). We trained a student expert model based on two teacher expert models (tasks 1 and 2), each separately trained on the first two tasks in the sequence. The student expert model uses the same architecture as the teacher models and is trained without access to the original training data. To achieve this, we generate synthetic data approximating the data distributions on which the teacher models were initially trained, using Gaussian random variables. Next, we combine two in-domain models (tasks 1 and 2) into a single in-domain model, averaging their outputs with a weighting factor of 0.5. These fused models, which capture the knowledge from tasks 1 and 2, are then evaluated alongside models trained on task 3. The results show that our proposed method achieves an accuracy of 90.9% across these three tasks. Notably, when we combine the models of tasks 1 and 2, the accuracy increases to 93.1%. This experiment demonstrates that the approach is potentially scalable and effective for handling multiple tasks. It not only reduces the number of models that need to be maintained, but also improves overall performance.

6. Summary

We propose a task-conditioned ensemble-based method for continuously learning an existing expert model. The method introduces an in-domain model that provides membership information to dynamically combine different task expert models. Evaluation of the proposed approach across three experimental setups, each representing different levels of distribution shifts, demonstrates its effectiveness. Since the method does not alter the existing expert models—either through the training process or by adding new architecture—it facilitates the reuse of these models. In future work, we plan to apply this approach to other application areas.

References

- [1] Warsaw University of Technology, Poland. <http://zbum.ia.pw.edu.pl/EN/node/46>. 5
- [2] Rahaf Aljundi, Francesca Babiloni, Mohamed Elhoseiny, Marcus Rohrbach, and Tinne Tuytelaars. Memory aware synapses: Learning what (not) to forget. *European Conference on Computer Vision (ECCV)*, pages 139–154, 2018. 1, 2, 7
- [3] Jihwan Bang, Heesu Kim, YoungJoon Yoo, Jung-Woo Ha, and Jonghyun Choi. Rainbow memory: Continual learning with a memory of diverse samples. *Conference on Computer Vision and Pattern Recognition (CVPR)*, pages 8218–8227, 2021. 1, 2, 7
- [4] Steven Braun, Martin Mundt, and Kristian Kersting. Deep classifier mimicry without data access. *International Conference on Artificial Intelligence and Statistics (AISTATS)*, 238:4762–4770, 2024. 8
- [5] Markus M. Breunig, Hans-Peter Kriegel, Raymond T. Ng, and Jörg Sander. LOF: Identifying density-based local outliers. *ACM SIGMOD International Conference on Management of Data*, page 93–104, 2000. 4
- [6] Arslan Chaudhry, Marcus Rohrbach, Mohamed Elhoseiny, Thalaiyasingam Ajanthan, Puneet K. Dokania, Philip H. S. Torr, and Marc’Aurelio Ranzato. Continual learning with tiny episodic memories. *International Conference on Machine Learning (ICML)*, 2019. 2, 7
- [7] Priyanka Das et al. Iris liveness detection competition (LivDet-Iris)-the 2020 edition. *IEEE International Joint Conference on Biometrics (IJCB)*, pages 1–9, 2020. 5
- [8] Matthias De Lange et al. A continual learning survey: Defying forgetting in classification tasks. *IEEE Transactions on Pattern Analysis and Machine Intelligence (PAMI)*, pages 3366–3385, 2021. 1
- [9] Thang Doan, Seyed Iman Mirzadeh, and Mehrdad Farajtabar. Continual learning beyond a single model. *arXiv*, abs/2202.09826, 2023. 1, 2
- [10] Alexey Dosovitskiy et al. An image is worth 16x16 words: Transformers for image recognition at scale. *International Conference on Learning Representations (ICLR)*, 2021. 2, 4
- [11] Arthur Douillard, Alexandre Ramé, Guillaume Couairon, and Matthieu Cord. Dytox: Transformers for continual learning with dynamic token expansion. *Conference on Computer Vision and Pattern Recognition (CVPR)*, pages 9275–9285, 2022. 1, 2
- [12] Mehrdad Farajtabar, Navid Azizan, Alex Mott, and Ang Li. Orthogonal gradient descent for continual learning. *International Conference on Artificial Intelligence and Statistics (AISTATS)*, pages 3762–3773, 2020. 1, 2
- [13] Geoffrey Hinton, Oriol Vinyals, and Jeff Dean. Distilling the knowledge in a neural network. *NIPS Deep Learning Workshop*, 2014. 8
- [14] Yen-Chang Hsu, Yen-Cheng Liu, Anita Ramasamy, and Zsolt Kira. Re-evaluating continual learning scenarios: A categorization and case for strong baselines. *NIPS Continual Learning Workshop*, 2018. 2, 6, 7
- [15] Zhiqiang Hu, Lei Wang, Yihuai Lan, Wanyu Xu, Ee-Peng Lim, Lidong Bing, Xing Xu, Soujanya Poria, and Roy Ka-Wei Lee. LLM-Adapters: An adapter family for parameter-efficient fine-tuning of large language models. *Empirical Methods in Natural Language Processing (EMNLP)*, 2023. 1
- [16] Adam Ibrahim, Benjamin Thérien, Kshitij Gupta, Mats L. Richter, Quentin Anthony, Timothée Lesort, Eugene Belilovsky, and Irina Rish. Simple and scalable strategies to continually pre-train large language models. *Transactions on Machine Learning Research (TMLR)*, 2024. 1, 2
- [17] Khurram Javed and Martha White. Meta-learning representations for continual learning. *Advances in Neural Information Processing Systems (NeurIPS)*, 32, 2019. 2
- [18] K. J. Joseph and Vineeth N. Balasubramanian. Meta-consolidation for continual learning. *Advances in Neural Information Processing Systems (NeurIPS)*, 2020. 2
- [19] Haeyong Kang, Rusty John Lloyd Mina, Sultan Rizky Hikmawan Madjid, Jaehong Yoon, Mark Hasegawa-Johnson, Sung Ju Hwang, and Chang D. Yoo. Forget-free continual learning with winning subnetworks. *International Conference on Machine Learning (ICML)*, 162:10734–10750, 2022. 2
- [20] Ta-Chu Kao, Kristopher Jensen, Guido van de Ven, Alberto Bernacchia, and Guillaume Hennequin. Natural continual learning: success is a journey, not (just) a destination. *Advances in Neural Information Processing Systems (NeurIPS)*, 34:28067–28079, 2021. 1, 2, 7
- [21] James Kirkpatrick et al. Overcoming catastrophic forgetting in neural networks. *Proceedings of the National Academy of Sciences (PNAS)*, 114(13):3521–3526, 2017. 2, 7
- [22] Soochan Lee, Junsoo Ha, Dongsu Zhang, and Gunhee Kim. A neural dirichlet process mixture model for task-free continual learning. *International Conference on Learning Representations (ICLR)*, 2020. 2, 7
- [23] Zhizhong Li and Derek Hoiem. Learning without forgetting. *IEEE transactions on Pattern Analysis and Machine Intelligence (PAMI)*, 40(12):2935–2947, 2017. 1, 2, 7
- [24] Guoliang Lin, Hanlu Chu, and Hanjiang Lai. Towards Better Plasticity-Stability Trade-off in Incremental Learning: A Simple Linear Connector. *Conference on Computer Vision and Pattern Recognition (CVPR)*, 2022. 1, 2
- [25] Yuang Liu, Wei Zhang, Jun Wang, and Jianyong Wang. Data-free knowledge transfer: A survey. *ArXiv*, abs/2112.15278, 2021. 8
- [26] David Lopez-Paz and Marc’Aurelio Ranzato. Gradient episodic memory for continual learning. In *International Conference on Neural Information Processing Systems*, page 6470–6479, 2017. 7
- [27] David Lopez-Paz and Marc’Aurelio Ranzato. Gradient episodic memory for continual learning. *Advances in Neural Information Processing Systems (NeurIPS)*, 30, 2017. 2, 6, 7
- [28] Divyam Madaan, Jaehong Yoon, Yuanchun Li, Yunxin Liu, and Sung Ju Hwang. Rethinking the representational continuity: Towards unsupervised continual learning. *International Conference on Learning Representations (ICLR)*, 2021. 2

- [29] Imad Eddine Marouf, Subhankar Roy, Enzo Tartaglione, and Stéphane Lathuilière. Weighted ensemble models are strong continual learners. *European Conference on Computer Vision (ECCV)*, 2024. 1, 2
- [30] José Mauricio, Inês Domingues, and Jorge Bernardino. Comparing vision transformers and convolutional neural networks for image classification: A literature review. *Applied Sciences*, 13(9), 2023. 3
- [31] Seyed Iman Mirzadeh, Mehrdad Farajtabar, Dilan Gorur, Razvan Pascanu, and Hassan Ghasemzadeh. Linear mode connectivity in multitask and continual learning. *International Conference on Learning Representations (ICLR)*, 2020. 2
- [32] Jose G. Moreno-Torres, Troy Raeder, Roc̃Ao Alaiz-Rodr̃Aguez, Nitesh V. Chawla, and Francisco Herrera. A unifying view on dataset shift in classification. *Pattern Recognition (PR)*, 45(1):521–530, 2012. 1
- [33] Quang Pham, Chenghao Liu, and Steven C.H. Hoi. Dualnet: continual learning, fast and slow. *International Conference on Neural Information Processing Systems (NIPS)*, 2021. 1, 2
- [34] Ameya Prabhu, Philip H. S. Torr, and Puneet K. Dokania. Gdumb: A simple approach that questions our progress in continual learning. *European Conference on Computer Vision (ECCV)*, pages 524–540, 2020. 2, 7
- [35] Jathushan Rajasegaran, Munawar Hayat, Salman H Khan, Fahad Shahbaz Khan, and Ling Shao. Random path selection for continual learning. *Advances in Neural Information Processing Systems (NeurIPS)*, 32, 2019. 2
- [36] Rahul Ramesh and Pratik Chaudhari. Model zoo: A growing brain that learns continually. *International Conference on Learning Representations (ICLR)*, 2022. 1, 2
- [37] Hippolyt Ritter, Aleksandar Botev, and David Barber. Online structured laplace approximations for overcoming catastrophic forgetting. *Advances in Neural Information Processing Systems (NeurIPS)*, 31, 2018. 2, 7
- [38] Andrei A. Rusu, Neil C. Rabinowitz, Guillaume Desjardins, Hubert Soyer, James Kirkpatrick, Koray Kavukcuoglu, Razvan Pascanu, and Raia Hadsell. Progressive neural networks. *ArXiv*, abs/1606.04671, 2016. 2
- [39] Jonathan Schwarz et al. Progress & compress: A scalable framework for continual learning. *International Conference on Machine Learning (ICML)*, pages 4528–4537, 2018. 2, 7
- [40] Renu Sharma and Arun Ross. D-NetPAD: An explainable and interpretable iris presentation attack detector. *IEEE International Joint Conference on Biometrics (IJCB)*, pages 1–10, 2020. 4, 5
- [41] Y Shi, K Zhou, J Liang, Z Jiang, J Feng, P Torr, S Bai, and VYF Tan. Mimicking the oracle: an initial phase decorrelation approach for class incremental learning. *Conference on Computer Vision and Pattern Recognition (CVPR)*, pages 16701–16710, 2022. 2
- [42] Hanul Shin, Jung Kwon Lee, Jaehong Kim, and Jiwon Kim. Continual learning with deep generative replay. *Advances in Neural Information Processing Systems (NeurIPS)*, 30, 2017. 2, 6, 7
- [43] Sidak Pal Singh and Martin Jaggi. Model fusion via optimal transport. *Advances in Neural Information Processing Systems (NeurIPS)*, 33:22045–22055, 2020. 8
- [44] George Stoica, Daniel Bolya, Jakob Bjorner, Taylor Hearn, and Judy Hoffman. Zipit! merging models from different tasks without training. *International Conference on Learning Representations (ICLR)*, 2024. 8
- [45] Guido M Van de Ven and Andreas S Tolias. Generative replay with feedback connections as a general strategy for continual learning. *arXiv*, abs/1809.10635, 2018. 2, 6, 7
- [46] Guido M. van de Ven and Andreas S. Tolias. Three scenarios for continual learning. *Advances in Neural Information Processing Systems (NeurIPS) workshop*, 2018. 2, 6
- [47] Laurens Van der Maaten and Geoffrey Hinton. Visualizing data using t-SNE. *Journal of Machine Learning Research (JMLR)*, 9(11), 2008. 8
- [48] Ashish Vaswani, Noam Shazeer, Niki Parmar, Jakob Uszkoreit, Llion Jones, Aidan N Gomez, Łukasz Kaiser, and Illia Polosukhin. Attention is all you need. *Advances in Neural Information Processing Systems (NeurIPS)*, 30, 2017. 2
- [49] Liyuan Wang, Xingxing Zhang, Qian Li, Jun Zhu, and Yi Zhong. CoSCL: Cooperation of small continual learners is stronger than a big one. *European Conference on Computer Vision (ECCV)*, pages 254–271, 2022. 2
- [50] Liyuan Wang, Xingxing Zhang, Hang Su, and Jun Zhu. A comprehensive survey of continual learning: Theory, method and application. *IEEE Transactions on Pattern Analysis and Machine Intelligence (PAMI)*, 46(8):5362–5383, 2024. 1, 2
- [51] Runqi Wang, Yuxiang Bao, Baochang Zhang, Jianzhuang Liu, Wentao Zhu, and Guodong Guo. Anti-retroactive interference for lifelong learning. *European Conference on Computer Vision (ECCV)*, pages 163–178, 2022. 6, 7
- [52] Tz-Ying Wu, Gurumurthy Swaminathan, Zhizhong Li, Avinash Ravichandran, Nuno Vasconcelos, Rahul Bhotika, and Stefano Soatto. Class-incremental learning with strong pre-trained models. *Conference on Computer Vision and Pattern Recognition (CVPR)*, 2022. 1, 2
- [53] Yue Wu, Yan-Jia Chen, Lijuan Wang, Yuancheng Ye, Zicheng Liu, Yandong Guo, and Yun Fu. Large scale incremental learning. *Conference on Computer Vision and Pattern Recognition (CVPR)*, 2019. 2, 7
- [54] Ziyang Wu, Christina Baek, Chong You, and Yi Ma. Incremental learning via rate reduction. *Conference on Computer Vision and Pattern Recognition (CVPR)*, 2021. 2
- [55] Mengqi Xue, Haofei Zhang, Jie Song, and Mingli Song. Meta-attention for vit-backed continual learning. *Conference on Computer Vision and Pattern Recognition (CVPR)*, pages 150–159, 2022. 1, 2
- [56] David Yambay et al. LivDet iris 2017—iris liveness detection competition 2017. *IEEE International Joint Conference on Biometrics (IJCB)*, pages 733–741, 2017. 4, 5
- [57] G. Zeng, Y. Chen, B. Cui, and S. Yu. Continual learning of context-dependent processing in neural networks. *Nature Machine Intelligence*, 1:364–372, 2019. 2, 7
- [58] Friedemann Zenke, Ben Poole, and Surya Ganguli. Continual learning through synaptic intelligence. *International Conference on Machine Learning (ICML)*, pages 3987–3995, 2017. 2, 7